

Surface-tip interactions in noncontact atomic-force microscopy on reactive surfaces: Si(111)

Rubén Pérez

Departamento de Física Teórica de la Materia Condensada, Universidad Autónoma de Madrid, E-28049, Madrid, Spain

Ivan Štich

*JRCAT, Angstrom Technology Partnership, 1-1-4 Higashi, Tsukuba, Ibaraki 305, Japan
and Slovak Technical University, Department of Physics, Ilkovičova 3, SK-812 19 Bratislava, Slovakia*

Michael C. Payne

Theory of Condensed Matter, Cavendish Laboratory, University of Cambridge, Madingley Road, Cambridge CB3 0HE, United Kingdom

Kiyoyuki Terakura

*JRCAT, National Institute for Advanced Interdisciplinary Research, 1-1-4 Higashi, Tsukuba, Ibaraki 305, Japan
and Institute of Industrial Science, University of Tokyo, Roppongi, Minato-ku, Tokyo 106, Japan*

(Received 9 March 1998; revised manuscript received 11 May 1998)

Total-energy pseudopotential calculations are used to study the imaging process in noncontact atomic-force microscopy on Si(111) surfaces. At the distance of closest approach between the tip and the surface, there is an onset of covalent chemical bonding between the dangling bonds of the tip and the surface. Displacement curves and lateral scans on the surface show that this interaction energy and force are comparable to the macroscopic Van der Waals interaction. However, the covalent interaction completely dominates the force gradients probed in the experiments. Hence, this covalent interaction is responsible for the atomic resolution obtained on reactive surfaces and it should play a role in improving the resolution in other systems. Our results provide a clear understanding of a number of issues such as (i) the experimental difficulty in achieving stable operation, (ii) the quality of the images obtained in different experiments and the role of tip preparations and (iii) recently observed discontinuities in the force gradient curves. [S0163-1829(98)08336-2]

I. INTRODUCTION

The atomic force microscope¹ (AFM) has developed as a tool which allows routine investigation of surface structures by probing the spatial variations of the forces between a tip and a surface. In its usual mode of operation, the *constant force mode*, the surface structure is determined by measuring the variation of the tip height which yields a constant force as the tip scans across the surface. Unlike the scanning tunneling microscope (STM), where the images reflect the electronic band structure around the Fermi level, the atomic tip-surface forces probed by AFM are, at least in principle, more directly related to the surface atomic structure and hence should also be simpler to interpret. However, experimental problems with controlling the repulsive forces at the apex atom resulting from the long-range attractive forces acting on the tip as well as the interpretation of the complex nature of the surface-tip forces have made the progress in AFM of well characterized surfaces in ultrahigh vacuum unexpectedly slow. In particular, images taken in the *contact mode* rarely show individual surface defects, which are routinely observed with STM, which raises the question of whether the AFM is really capable of atomic resolution.

Only recently have Giessibl,² Kitamura and Iwatsuki,³ and Ueyama *et al.*⁴ demonstrated that *noncontact* AFMs operating in the attractive regime on reactive surfaces could produce true atomic resolution. These experiments used an alternative ac mode of imaging to reduce the effect of the long-range attractive forces. In this mode the tip moves in and out of the interaction region during each oscillation

cycle. In its original version, the *frequency shift mode*, the frequency of a tip oscillating at its eigenfrequency ω is modified by an amount $\Delta\omega$, as a result of the change of the effective cantilever spring constant k by Δk due to the tip-sample interaction. Δk is equal to the gradient of the force between the tip and the surface $(\partial F_{\text{tip-sample}}/\partial z)$, and Δk and $\Delta\omega$ are related by

$$\frac{\Delta\omega}{\omega} \propto \frac{\Delta k}{k}. \quad (1)$$

Hence, in this mode of operation the experiments probe the force gradients and a scan at a constant $\Delta\omega$ generates a map of a constant average force gradient. This technique was successfully used to image a number of reactive semiconductor surfaces. Typically, these experiments use stiffer cantilevers ($\sim 15\text{--}50$ N/m) than those used in contact mode experiments (< 1 N/m) with tips of radius < 150 Å etched from Si with the estimated closest approach to the surface of ~ 5 Å and the attractive force, at that point, ~ -0.15 nN.² For example, on Si(111)- 7×7 a clear image of the unit cell with its twelve adatoms has been obtained,^{2,5} on Si(001)- 2×1 the individual dimer atoms as well as an S_B step and even the A, B, C defects could be resolved,⁵ as was the atomic structure of the InP(110)- 1×1 surface.⁶

Force gradient detection has also been combined with standard STM measurements.^{7,8} Simultaneous measurements of the resonance frequency shift of the cantilever and the mean tunneling current from the tip showed that stable imaging with true atomic resolution is only possible over a restricted range of tip-sample distances. Using the averaged

tunnel current instead of the average force gradient as the feedback parameter, stable operation was achieved and atomic images of the Si(111)- 7×7 reconstruction in the vicinity of a monoatomic step were obtained.

This technique was later modified by allowing for oscillation *amplitude damping* when the tip comes in close proximity to the surface.^{9–11} This technique provided very clear images of the Si(111)- 7×7 surface, of quality comparable to that of an STM image, showing differences between inequivalent adatoms. The observed contrast, however, varies between different experiments: the center adatoms appear 0.13 Å higher than the corner adatoms in Ref. 9, where a metallic tip was used, while in Refs. 10 and 11, using a Si tip, the contrast is reversed, with the corner adatoms appearing higher than the center adatoms.

It has also been demonstrated that the jump to contact may be avoided by applying a feedback control and then the tip-surface forces and energies as a function of tip-surface distance can be mapped out using a technique that could be called *AFM spectroscopy*.¹²

All of the experiments outlined above raise a number of questions, such as the detailed nature of the surface-tip interaction at the distance of closest approach [estimated to be ~ 5 Å, (Ref. 2)], which only theory can address. In particular, very little is known about the mechanism that provides atomic resolution in these experiments or about the variations between images taken under different experimental conditions or even between different parts of the same image. To address some of these questions we have performed an extensive theoretical study of the tip-surface interactions, taking the Takayanagi-reconstructed Si(111) surface¹³ as a typical representative of the reactive surfaces probed in the experiments. A theoretical description of the phenomena that are relevant to AFM must properly account for the variation of the force with varying tip-surface distance z . At large separations the tip-surface interaction will be dominated by the long-range Van der Waals (VdW) dispersive forces while at small separations the short-range quantum-chemical forces have to be considered. To describe the latter we use density functional theory (DFT),¹⁴ which has been shown to provide a reliable description of the surface-tip interaction at distances of a few interatomic distances.^{15,16} For the long-range forces we adopt a model based on the VdW interaction between macroscopic bodies.¹⁷ Using this description of the interaction we study in detail both vertical as well as horizontal scans, hereafter referred to as displacement curves and lateral scans, respectively. Our work has a rather direct bearing on the noncontact frequency shift AFM experiments^{2–8} and on the AFM spectroscopy experiments.¹² Their relevance to the amplitude damping experiments⁹ is less obvious, but differences in the response of the adatoms, such as those discussed below, are a possible mechanism to explain the observed contrast in this imaging mode. Because of the computational cost, accurate *ab initio* studies, similar in spirit to those presented here, exist only for Al surfaces with a high degree of symmetry.^{15,16}

Our previous work, presented in Ref. 18, pointed out that the covalent chemical interaction between the dangling bonds of the adatoms on the surface and of the apex atom in the tip do play an important role in the quality of the images obtained in noncontact AFM. We showed that, even for dis-

tances as large as ~ 5 Å, that was the estimated distance of closest approach in the earlier experiments, this interaction generates forces that are of comparable magnitude to the VdW tip-surface interaction but, more importantly, this covalent chemical interaction dominates the force gradients probed in noncontact AFM. Hence, it is this interaction that provides a mechanism for atomic resolution imaging of reactive surfaces.

In the present work, extensive simulations are used to completely characterize that covalent interaction for the case of the Si(111)- 7×7 reconstruction, the system for which most of the experiments have been done. These simulations include displacement curves over several relevant points of the unit cell and lateral scans at a constant height of 5 Å over a large area of the surface unit cell. We present a detailed study of the variation of the force and the force gradients as a function of the tip-surface distance on the different adatoms and rest atoms. These results confirm that only the short-range chemical interaction is able to provide a variation of the force gradient across the surface that is large enough to achieve atomic resolution. They also show the important role of the relaxation of the atoms in the tip and the surface under the forces present. This atomic relaxation is responsible for the difference between the tip apex-surface atom distance and the tip displacement, which is the quantity accessible to the experiments. This difference has to be taken into account in the interpretation of AFM scans and also STM data. Special attention is paid to the possible accurate parametrization of our results for the tip-surface interaction using simple model potentials, such as the Morse and the Rydberg potentials. Such a parametrization would open the possibility of performing realistic simulations of the cantilever dynamics during noncontact AFM operation, still necessary to understand in a quantitative way the relation between force gradients and measured frequency shifts. Our lateral scans provide a direct relation between the main features of the AFM images and the structural and electronic properties of the surface. Particularly relevant are the charge-transfer processes among the dangling bonds and backbonds induced by the tip, which can be related to the changes in the relative contribution of the different dangling bonds to the states close to the Fermi energy due to the different interaction with the tip.

The rest of the paper is organized as follows. Section II describes the details of the model and computational techniques used, paying special attention to the characterization of the tip employed in our simulations. The convergence of these calculations with respect to various computational parameters is discussed in detail in Appendix A. The results of the simulations of displacement curves and the discussion of the atomic relaxation effects and the force gradient curves and fittings are included in Sec. III A. Lateral scans are presented in III B. Finally, in Sec. IV, our main findings are used to understand a number of experimental issues such as the difficulty in achieving stable operation, the relation between the quality of the images and the experimental conditions, with special emphasis on the role of the tip preparation, and the origin of the recently observed discontinuities in the force gradient curve.

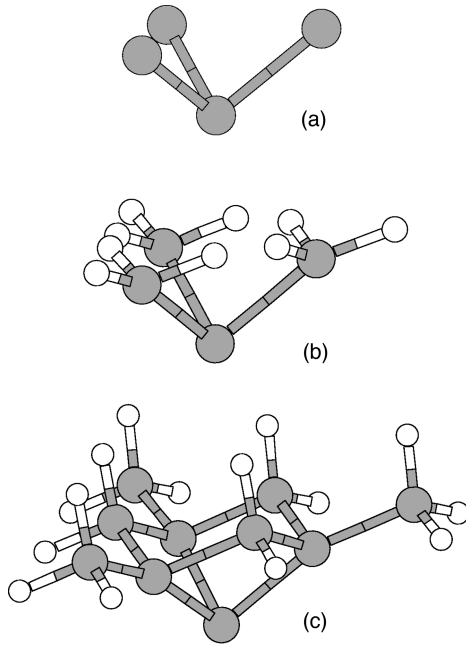


FIG. 1. Ball-and-stick model of the tips considered. (a) A 4 Si atom tip with dangling bonds of the atoms in the base unsaturated; (b) the same tip but the dangling bonds in the base are saturated by hydrogen atoms; (c) a 10 Si atom tip with the dangling bonds in the base saturated by hydrogen atoms.

II. MODEL AND SIMULATION TECHNIQUES

A. Short-range interactions

As mentioned in the previous section, in this work the short-range interactions between the AFM tip and the surface are modeled using DFT. Most of the calculations that will be presented were performed on the 5×5 member of the series

of Takayanagi reconstructions.¹³ While computationally more tractable than the experimentally observed 7×7 structure, it contains most of the features of the 7×7 structure, in particular, the adatoms and rest atoms. For testing purposes calculations have also been performed on the 3×3 structure. The system that we have considered is a supercell containing a Si(111) slab, two tips, one on each side of the Si slab and the vacuum region, with inversion symmetry imposed on the supercell. The slab consists of eight (111) planes and 200 Si atoms for the 5×5 reconstruction (68 for the 3×3), with the central two layers kept fixed to simulate the bulk crystal termination of the surface. The periodic images of the Si(111) slabs are four double layers apart, providing a vacuum region of at least 6.86 Å between the tips. The tips used in experiments are etched out of single-crystal Si.^{2,3,5,6} As the natural cleavage planes of Si are the (111) planes, we expect that the very end of the tip will be bounded by those planes. A natural question arises about the finite size of the tip to be used in the simulations. Within this model we considered three different tips, which are shown in Fig. 1. The reason for considering tips (a) and (b) separately even though they both contain four silicon atoms can be seen in Fig. 2, which shows the charge-density difference $\Delta\rho(\mathbf{r}) = \rho_{tip-b}(\mathbf{r}) - \rho_{tip-a}(\mathbf{r})$ on a plane through the tips. The saturation of the dangling bonds in the base of tip (b) changes the hybridization of the atom in the apex to close to the sp^3 hybrid of the bulk, leaving a dangling bond pointing out of the apex atom towards the surface. The third tip (c) with 10 Si atoms and the base dangling bonds saturated by hydrogen atoms, has a charge distribution in the apex region similar to tip (b).

In Ref. 18 we showed that although similar in the apex geometry, those differences in the charge density produced significantly different results for the interaction of the vari-

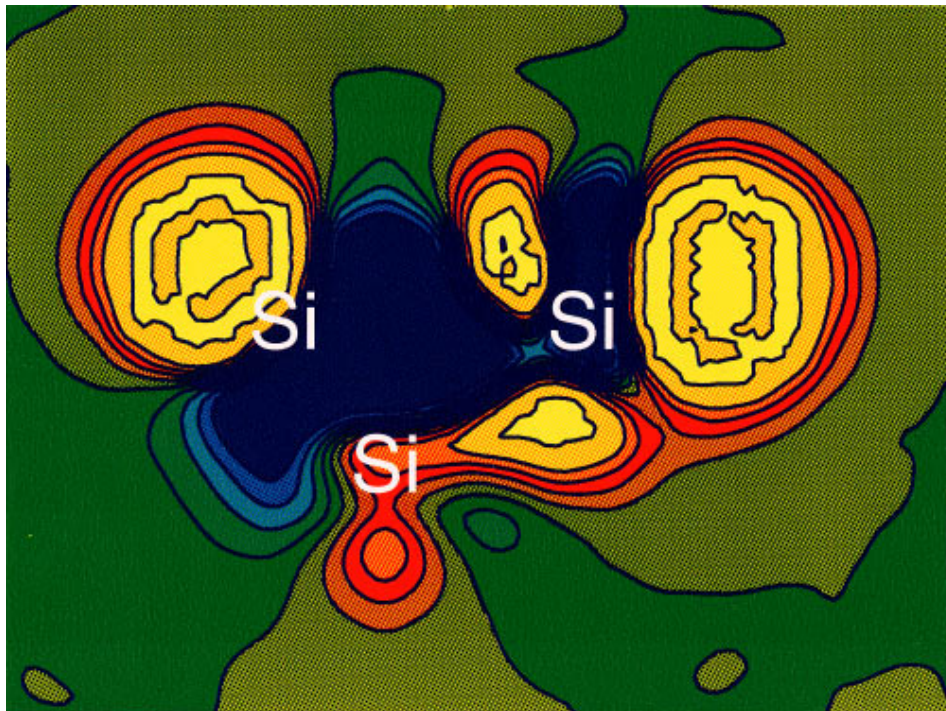


FIG. 2. (Color) Difference of the electronic charge densities between tip (b) and tip (a) of Fig. 1. Note the presence of a sp^3 -like dangling bond in (b) protruding out of the apex atom.

ous tips with the surface when we scan over an adatom in the faulted half of the 5×5 unit cell at a constant height of 5 \AA . We found that the total energy and normal force obtained for the two tips that have dangling bonds pointing towards the surface [tips (b) and (c) in Fig. 1] were very similar, and much larger than the values obtained for the unsaturated tip (a) (see Fig. 1 in Ref. 18 for details). These small differences between the 4 and 10 Si atom tips [tips (b) and (c), respectively] show that the short-range tip-surface interaction is completely dominated by the interaction of the dangling bond of the apex atom with the surface, and thus indicate that using tip (c) the simulations will be converged with respect to the size of the model used to represent the AFM tip. The results presented in the rest of the paper, except for some of the convergence tests in Appendix A, were obtained with the 10-atom tip with saturated dangling bonds in the base [tip (c) shown in Fig. 1].

The operation of the AFM in the lateral scanning mode was simulated in a stepwise, quasistatic manner by making small movements of the tip parallel to the surface at a constant height above the surface. At each step the atoms in the slab and the tip were allowed to relax to their equilibrium positions for that particular tip position. Similarly, for simulating the displacement curves the tip was moved from vacuum towards the surface with the atoms allowed to relax after each tip movement. In each case the Si atoms in the base of the tip and the H atoms attached to them, if these are present, are kept fixed in their positions after a tip displacement. These simulations are expected to provide an accurate description of both imaging modes since the motion of the AFM tip occurs on a much longer time scale than the atomic timescale. Similarly, finite-temperature effects are not expected to significantly modify the results as typical atomic frequencies (THz) are much larger than the tip oscillation frequency (kHz).

The energies and atomic forces were calculated within DFT (Ref. 14) in its plane-wave pseudopotential formulation.¹⁹ Optimized nonlocal pseudopotentials^{20,21} were used for silicon with the p and d components of the potential made very similar and optimized to make the pseudopotential rapidly convergent with respect to the cutoff energy in the plane-wave expansion. The pseudopotentials were applied in a separable form, taking the p component as reference and including only the s nonlocal component. The projection of this component was performed in real space.²² The Coulomb potential was used for the hydrogen atoms. The electronic orbitals were expanded at the Γ point of the Brillouin zone with a cutoff energy of 7 Ry. This set of parameters was found to yield highly accurate results for the total energies and vibrational frequencies for the 7×7 structure.^{23,24} We used the gradient corrected functional²⁵ for the exchange-correlation energy in the implementation of Ref. 26. The density functional was minimized with respect to both electronic and ionic degrees of freedom using conjugate gradient techniques.¹⁹ The convergence criteria were set to 5×10^{-5} eV/atom for the energies and to 1×10^{-2} eV/ \AA for the forces on the atoms. Since the Takayanagi-reconstructed Si(111) surface is metallic, the occupation of the electronic orbitals around the Fermi level was carefully checked. The simulations have been done using massively parallel computation.²⁷ The convergence of the

electronic-structure part of the simulation with respect to various computational parameters is discussed in Appendix A.

B. Long-range interactions

Dispersive VdW interactions are not correctly described by standard DFT. Recently a new long-range nonlocal exchange-correlation functional has been proposed to extend the applicability of DFT to the problem of physisorption at surfaces.²⁸ Although this prescription provides promising results for free-electron-like surfaces, its extension to semiconductor surfaces has not been developed yet. We have modeled the contribution of the VdW interaction to the total normal tip-surface force using the Hamaker summation method.¹⁷ The method is based on summation over the volume of the tip and sample of the asymptotic VdW pair potentials

$$W_{VdW}(r) = -\frac{C}{r^6}, \quad (2)$$

where the value of C depends on the tip and sample materials. The technique is applicable at distances sufficiently large to make the details of atomic structure unimportant. For example, for the VdW force acting on an atom over a polarizable flat surface of density ρ one obtains

$$F_{VdW}^{atom-surface}(r) = -\pi\rho C \frac{1}{r^4} = -\frac{A}{\pi\rho} \frac{1}{r^4}, \quad (3)$$

where A is the Hamaker constant, and r the atom-surface distance. We used this technique to estimate the normal forces and force gradients for the microscopic four Si atom tip [tip (a) of Fig. 1] and for a macroscopic spherical tip with the experimental curvature radius of $R=40 \text{ \AA}$,² where the interaction is given by

$$F_{VdW}^{sphere-surface}(r) = -\pi^2\rho^2CR \frac{1}{(r-R)^2} = -AR \frac{1}{(r-R)^2}, \quad (4)$$

with r being the distance from the surface to the center of the sphere. We use the Hamaker constant for the Si-Si interaction through air $A=1.865 \times 10^{-19} \text{ J}$.²⁹ We have considered the tip-surface distance in Eqs. (3) and (4) to be the normal distance between the tip and the highest adatoms, whose height is taken as a reference for the position of the flat surface with density $\rho(\text{Si}(111))$ in our calculations. Since the average height of the atoms in the surface is lower than the highest adatoms this model provides an upper bound for the interaction with a 5×5 reconstructed surface.

It could be argued that by using a sphere we are disregarding the contribution to the VdW interaction of the macroscopic parts of a tip which has a more realistic conical shape. A calculation similar to that for the sphere³⁰ shows that the cone-surface interaction is given by

$$F_{VdW}^{cone-surface}(r) = -A \frac{\tan^2\varphi}{6} \frac{1}{r}, \quad (5)$$

with r the distance from the surface to the apex of the cone, and φ the half-angle of aperture of the cone. An estimate using a cone with a half-angle of aperture of $\pi/4$ —using the same Hamaker constant—for the estimated distance of closest approach gives a force of 0.062 nN and a force gradient of 0.1 N/m, both of which are much smaller than the values of 0.50 nN and 2 N/m obtained for the sphere. Ciraci *et al.*¹⁵ found similar conclusions in their study of the VdW interaction between metallic tips and surfaces. They considered semi-infinite tips with conical and hemispherical ends and a cylindrical shank as a more realistic approximation to the tip shape. The Lifshitz formula for an atom interacting with a flat polarizable surface was integrated over the tip volume to obtain the total VdW interaction. Their results show that the hemispherical geometry gives contributions to the force and force gradient an order of magnitude larger than the ones obtained with the sharp conical tips (half-angle of aperture equal or less than $\pi/4$), in agreement with our model calculations.

Our calculations, as most of the work in Ref. 17, are based on the additivity of atomic contributions to calculate the total VdW force. As Hartmann³⁰ has shown, a more precise and conceptually satisfactory approach than that of Lifshitz³¹ gives the same results for the regime of small separations, where the nonretarded interaction is the dominant term.

Finally, it should be noticed that the possible error associated with a continuum description of the surface, instead of a detailed microscopic account of the discrete nature of the lattice in the areas closer to the tip, should be extremely small due to the long-range nature of the interaction, a generous upper bound being given by the order of magnitude of the VdW interaction between the 4 Si atom tip and the surface where the values of the force and the force gradient (-0.02 nN and 0.15 N/m, respectively, for a normal distance of 5 Å) are an order of magnitude smaller than the corresponding values for the macroscopic tip (-0.50 nN and 2 N/m, for the same normal distance).

III. RESULTS: SIMULATED AFM SCANS

A. Displacement curves: Tip-surface covalent bond and atomic relaxation

The results for the total energies³² and forces due to short- and long-range interactions are summarized in Figs. 3 and 4, respectively. In Fig. 3 and subsequent figures related to the short-range interaction, the results are plotted as a function of the “tip-surface distance,” which is defined as the difference in height between the unrelaxed tip apex and the highest adatom in the unrelaxed surface. In order to provide a direct comparison, results in Fig. 4 are also shown as a function of the analogous tip-surface distance; in this case, the difference in height between the surface of the sphere and the unrelaxed substrate highest adatoms, which defined the position of the flat surface in our model for the long-range interactions. With these definitions, variations in the tip-surface distance are then directly related to the relative displacements of tip and sample which are measured in the experiments.

The conclusion that emerges from the data in Figs. 3 and 4 is that only the short-range interaction at “near contact” distances (~ 3 –5 Å) is able to provide a variation in the

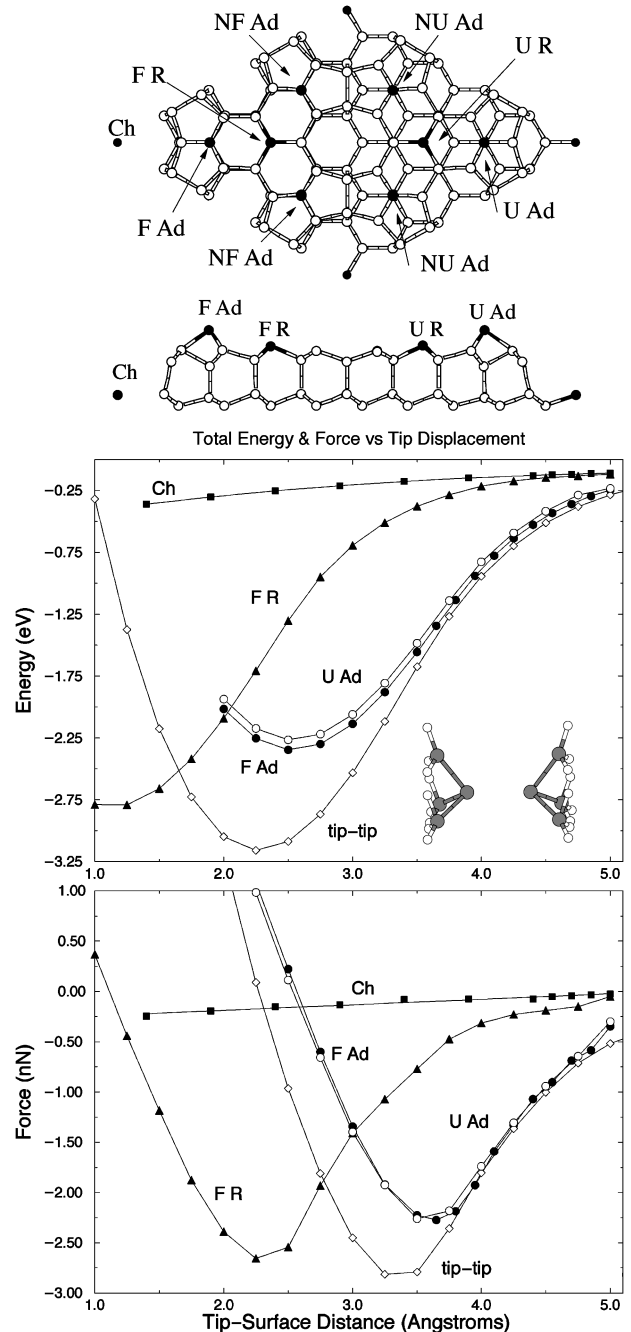


FIG. 3. Short-range interaction energy (middle panel) and normal force (bottom panel), as a function of the tip-surface distance, for tip (c) of Fig. 1 over corner hole atom (squares), over a rest atom (triangles) and the adatom on the long diagonal (black circles) in the faulted half of the unit cell, and over the adatom on the long diagonal in the unfaulted half (white circles). For comparison, the interaction between two tips [tip (b) of Fig. 1 as shown in the inset, white diamonds] is also shown. The top panel shows a ball-and-stick model of the 5×5 reconstruction, including a top view of the unit cell and a lateral view of the atoms close to the lattice plane along the long diagonal. The atoms with dangling bonds are marked: corner hole (Ch), faulted (F R) and unfaulted (U R) rest atoms, faulted diagonal (F Ad) and off-diagonal (NF Ad) adatoms, and unfaulted diagonal (U Ad) and off-diagonal (NU Ad) adatoms.

force gradient across the surface which is large enough to achieve atomic resolution. This short-range interaction is essentially an interaction between the surface adatom dangling

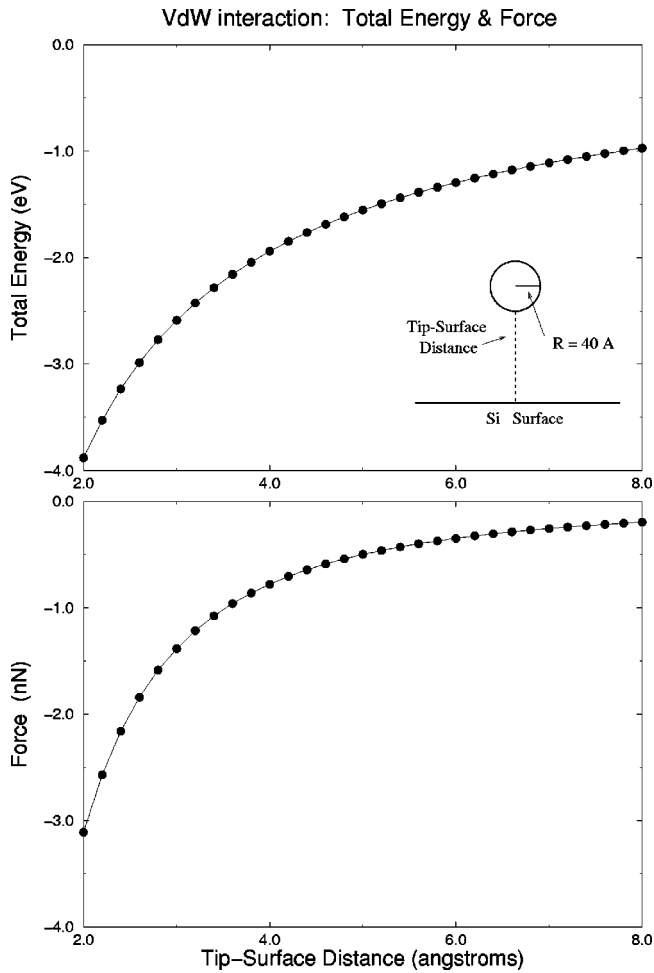


FIG. 4. Long-range van der Waals interaction energy (top panel) and force (bottom panel) as a function of the tip-surface distance for a macroscopic spherical tip of radius of 40 Å.

bond and tip apex dangling bond. This can be seen by comparing the curves for the scans over an adatom, a rest atom, and corner hole atom. This conclusion is further corroborated by results for a model system consisting of two interacting Si tips also shown in Fig. 3. These results, for both the total energy and the normal force, are very similar to those for the tip interacting with a surface adatom, apart from the striking differences in the position of the minima. The key to understanding the difference in the position of the minima is that when the atoms in the tip and the surface are allowed to relax under the forces present, the relative movement of the tip apex and the surface atoms is no longer the same as that of more distant parts of the tip and the sample. Our calculations show important relaxations even for a tip-surface distance of 5 Å, where the actual apex-adatom distance (apex-apex distance for the two interacting tips) after atomic relaxation reduces to 4.72 Å for the 5×5 reconstruction, 4.77 Å for the 3×3 reconstruction (see Appendix A for details), and 4.92 Å for the two Si tips. The effect of atomic relaxation becomes increasingly important as the tip and surface get closer. This point is illustrated in Fig. 5, where the distance between the apex tip atom and the surface atom just below the tip once relaxation is taken into account is shown as a function of the tip displacement (measured in terms of the tip-surface distance defined above). Considering the case of the tip dis-

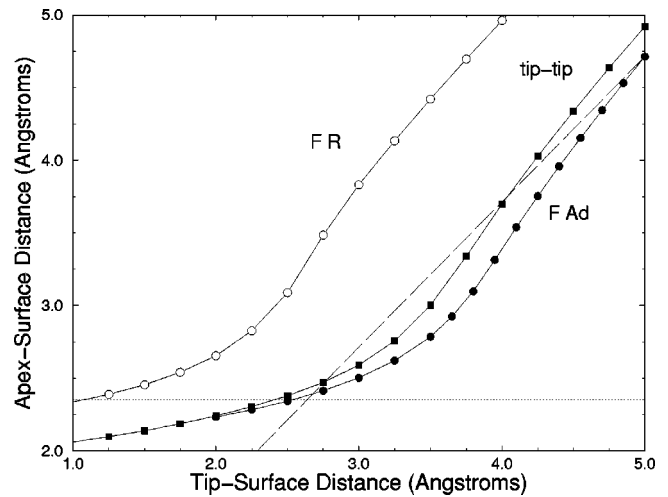


FIG. 5. Apex-adatom (apex-rest atom) distance as a function of tip displacement for tip (c) of Fig. 1 over a diagonal adatom (black circles) and a rest atom (white circles) in the faulted half of 5×5 reconstruction. The apex-apex distance for the interaction between two tips [tip (b) of Fig. 1 is also shown (squares)]. The dashed line shows the apex-adatom distance for the tip (c) over the adatom for a rigid displacement of the tip if no relaxation were allowed starting from the tip configuration at 5 Å. The horizontal dotted line corresponds to the nearest-neighbor distance in bulk Si.

placement over one of the adatoms as an example and taking the relaxed configuration at 5 Å as the starting point, if no further relaxation were present the apex-adatom distance would follow the dashed line shown in Fig. 5. It can be clearly seen that the real apex-adatom distance rapidly deviates from that linear behavior due to the relaxation of both the tip and surface atoms. Differences between the curves thus reflect the different atomic relaxations due to the different bonding of the atoms to the surface on the various systems considered. In all cases the minimum in the total energy (and zero in the normal force) corresponds to the tip position where the apex-surface atom distance (apex-apex distance) is roughly equal to 2.35 Å, which is marked by the horizontal dotted line in Fig. 5, the Si-Si nearest-neighbor distance in bulk Si. This difference between the apex-surface atom distance and the tip displacement, which is the quantity accessible to the experiments, should be taken into account not only in the AFM scans but also in the interpretation of STM data. Similar effects occur in the STM and have been invoked to explain the falloff in corrugation on Cu surfaces³³ and the constant value of the apparent barrier height at small tunnel resistances for several metallic surfaces.³⁴

The vertical scan over the rest atom shows a similar behavior to the scan over the adatom but the minima in both the total energy and normal force are displaced by around 1.25 Å, which is roughly the difference in height (1.12 Å) between the adatom and rest atom in the 5×5 reconstruction. The minimum in the total energy also corresponds to a distance between the tip apex atom and the rest atom equal to 2.35 Å. As the tip approaches the surface the rest atom moves up towards the tip apex until the tip-surface distance is roughly equal to 2.5 Å, close to the point where the maximum of the normal force is reached and the curvature of the apex-adatom distance versus tip-surface distance changes sign (see Fig. 5). The same behavior was found in the ada-

tom scan. In fact, if the rest atom curve in Fig. 5 is displaced in the horizontal direction by 1.25 Å, it overlaps almost perfectly with the one for the adatom.

The displacement curves discussed above were made over atoms on the faulted half of the unit cell. Results for the unfaulted half are very similar for both the total energy and the normal force, as the comparison between the scans over the faulted and the unfaulted adatom shows (see Fig. 3), and for this reason they will not be discussed further.

It was already pointed out in Ref. 18 that the covalent character of the short-range dangling bond interaction persisted at least up to a surface-tip distance of ~ 5 Å. The charge-density difference between the surface with the tip at a distance of 5 Å over one of its adatoms and a superposition of the charge densities of an isolated surface and tip (see Fig. 2 in Ref. 18) showed a pronounced charge transfer to the adatom dangling bond under the tip from the dangling bond on the rest atom and from the backbond. It should be noticed that a similar reverse charge transfer has been experimentally observed after chemisorption of molecules on the Si(111)- 7×7 surface.³⁵ This accumulation of charge in the adatom dangling bond (notice that the dangling bond in the tip has already one electron) is precisely what we expect at the onset of the formation of a covalent bond between the tip and the surface. The work presented here provides more evidence of the covalent character of this interaction. In particular, the fact that this is not just a polarization effect induced by the tip on the surface states but the onset of real covalent bonding is further confirmed by the spatial distribution of the charge density of the highest occupied electronic states, which clearly show that they are a bonding combination of the original dangling bond states in both the apex atom and the adatom (see the discussion about the character of the states around the Fermi energy at the end of Sec. III B and Fig. 13). Further support comes from the study of the formation of this bond as the tip approaches the adatom. The charge density difference shown in Fig. 6 for a tip-surface distance of 3.5 Å very much resembles the one in Fig. 1 in Ref. 18, except for the increase in the charge transferred to the adatom. The concept of chemical reactivity between the tip and the surface¹⁸ was recently invoked to explain the difference in the contrast between inequivalent adatoms on the Si(111)- 7×7 surface in the amplitude damping experiments.⁹

In order to perform simulations of the cantilever dynamics under the conditions used in noncontact AFM it would be desirable to have a simple but accurate description of the tip-surface interaction. Morse potentials are known to provide a reasonable description of covalent bonding in a diatomic molecule through a simple analytical function:

$$V(r) = V_0 \left\{ \left[1 - \exp\left(-2b \frac{r - R_c}{R_c}\right) \right]^2 - 1 \right\}, \quad (6)$$

where $V(r)$ represents the total bonding energy as a function of the interatomic distance r , and V_0 , b , and R_c are parameters that define the strength and range of the bonding interaction. Due to their simplicity, Morse potentials have been used in different contexts, including AFM simulations,³⁶ to simulate bonding interactions. We have also considered other functional dependencies used to fit total-energy curves,

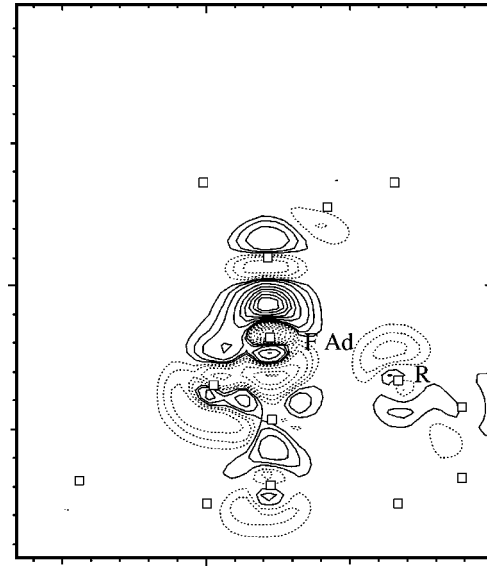


FIG. 6. Charge-density difference between the self-consistent electronic density of the interacting system and the superposition of the densities of the isolated tip and surface. The plot is taken on a plane perpendicular to the surface along the long diagonal in the faulted half of the unit cell. The tip is on top of the F Ad. The tip-surface distance is 3.5 Å. The squares indicate the position of the Si atoms in that plane both in the tip and in the Si surface. The solid (dotted) lines indicate an increase (decrease) of electronic charge; the contours correspond to ± 0.4 , ± 1 , ± 2 (as in Fig. 2 in Ref. 18), ± 4 , ± 6 , ± 8 , ± 10 , ± 12 , ± 14 and $\pm 16 \times 10^{-2}$ electrons/Å³. Notice the transfer of charge to the adatom dangling bond from the backbond and the dangling bond in the F R.

like the Rydberg function,³⁷ $V(r) = -V_0[1 + b(r - R_c)] \exp[-b(r - R_c)]$. The results obtained for the fits with this potential are very similar to the ones presented below for the Morse potential, and for this reason they will not be discussed further.

We have tried to fit our total-energy curves for the short-range tip-surface interaction and the interaction between the two tips shown in Fig. 3 with a Morse potential, taking r as the tip-surface distance and V_0 , b , and R_c as fitting parameters. However, it has not been possible to find a good fit for both the attractive and the repulsive parts of the interaction, and the fits obtained taking just the attractive part and few points in the repulsive region close to the minimum provide a very poor fit to the calculated force derivatives. Considering the differences between the tip-surface distance and the apex-surface atom distance when relaxation is taken into account as discussed above, and the fact that the Morse potential should describe the interaction of two atoms as a function of their real interatomic distance, we have also tried a fit taking r as the apex-surface atom distance. Although we obtained a little improvement, the quality of the fit was still far from satisfactory.

A direct fit to the calculated forces using the derivative of the Morse potential, taking r as the real apex-surface atom distance proved to be much more successful. The fits for the tip-adatom, tip-rest atom, and tip-tip force are shown in Fig. 7. It should be noticed that although the fit is done with the real interatomic distance, the plot is presented with respect to the corresponding tip-surface distance defined above. These

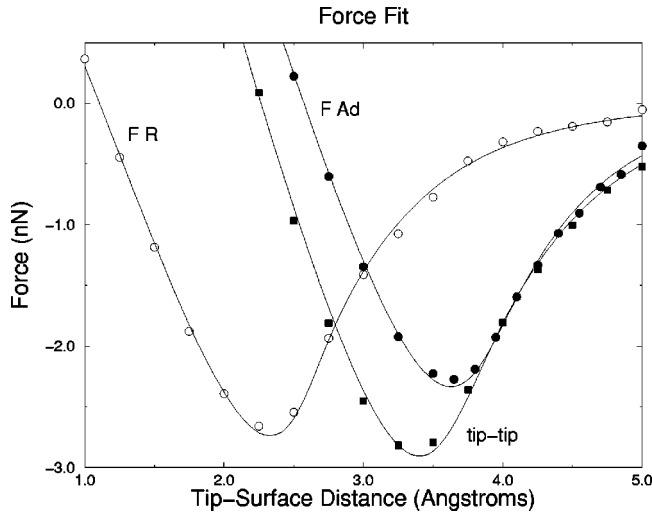


FIG. 7. Morse fits to the normal force for the tip-diagonal adatom (black circles) and the tip-rest atom (white circles). The fit for the tip-tip interaction (squares) is shown for comparison. In each case the symbols correspond to the calculated values of the force while the lines represent the fit.

fits reproduce the behavior of the force close to its minimum, and the integration of those curves provide a reasonable, although not very accurate, description of the total energy for the different systems. The quality of the fits deteriorates if we try to include more fitting points in the repulsive part of the force, showing that, as one can expect, the tip-surface interaction deviates from the pure “diatomic” case as the tip approaches the surface and the response of the adatom or the rest atom becomes more influenced by the atoms in the layers below. It must be noted that good fits are only obtained when we use the real apex-surface atom distance, further confirming the importance of the relaxation effects described above. Typical values for the fitting parameters are shown in Table I. The quality of the fits for the force and the total energy seems to be better in the case of the interaction of the two tips than for the tip-surface interaction. In particular, the fits for the adatom and rest atom on the 5×5 reconstruction do not reproduce the calculated values for the largest distances (around 5 \AA), which are well described in the case of the tip-tip interaction. The convergence tests discussed in Appendix A seem to rule out large inaccuracies in our calculated forces and one can speculate as to the origin of these differences. One possible explanation is simply that a Morse-type function is too simple to describe the details of the interaction, and a fit that tends to better reproduce the area with larger values around the minimum will fail to describe the behavior accurately for large distances. In this respect,

TABLE I. Parameters obtained in the fit of the forces with the derivative of the Morse potential [Eq. (6)] for tip (c) interacting with an adatom and a rest atom on a Si(111)- 5×5 surface, and for the interaction between two tips [tip (b) in Fig. 1].

	V_0 (eV)	b	R_c (\AA)
Adatom	2.273	1.497	2.357
Rest atom	2.636	1.526	2.357
Two tips	3.094	1.328	2.292

the tip-tip interaction should be easier to describe as the charge in the dangling bonds of the two tips is the same over the whole distance range. There are no large changes in the eigenstate distribution around the Fermi level since only the states associated with the two unsaturated dangling bonds are present. The situation is much more complicated for the tip-surface interaction where several states associated with the different dangling bonds on the surface are close to the Fermi level. In this case, charge piles up in the dangling bond interacting with the tip and is depleted from other areas, the amount of charge depending on the strength of the interaction between the adatom- and tip-dangling bonds. This is described in detail at the end of next section. In summary, the fitting process provides further support to the central role of covalent bonding in the tip-surface interaction, but, at the same time, it reveals some of the subtle differences from a simple model of diatomic bonding.

As pointed out in the Introduction, force gradients play a crucial role in noncontact AFM. The force gradients are not a direct output of our total-energy calculations, but we can calculate them from the force versus distance curves discussed above. The most accurate way to do this would be to take a numerical derivative of the calculated force curve over the whole distance range. However, that would require a finer grid than the one we can afford due to the computational cost of the calculations. One possible solution is to take a derivative of the force fits obtained above. Figure 8 compares the force gradients for the tip-tip, tip-adatom, and tip-rest atom interaction, obtained as a derivative of the corresponding force fits, with the force gradients associated with the long-range VdW interaction for the macroscopic tip, obtained as well as a derivative of Eq. (4). This figure clearly shows the similarities between all the covalent bonding interactions as opposed to the VdW interaction. Obviously, the values for the force gradients are not very accurate for larger distances due to the limitations of the fits. Our force fits tend to underestimate the force gradients for large distances when

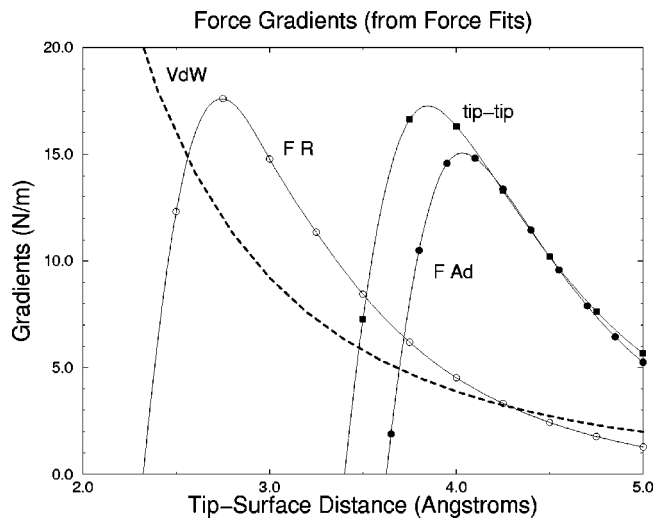


FIG. 8. Force gradients for the the tip-diagonal adatom (black circles), the tip-rest atom (white circles), and the tip-tip (squares) interaction (obtained as a derivative of the corresponding force fits). Force gradients associated with the long-range VdW interaction for the macroscopic spherical tip of radius 40 \AA are indicated by the dashed line.

compared to the values obtained from a numerical derivative on a finer grid. The force gradient on the faulted adatom at a distance of 5 Å obtained from the calculation of the force on a fine grid centered at that distance and the use of a numerical derivative is almost a factor of 2 larger than the one obtained from the force fit (see Table I in Ref. 18). The results in Fig. 8 clearly show that the covalent bonding interaction dominates the force gradients that cause the frequency shifts used to create the experimental images. We note that similar results have also been obtained for the 3×3 surface.³⁸

B. Lateral scans

The conclusion from the simulations of the vertical scans is that the tip-surface force and force gradients for distances larger than 4 Å are only significant close to the adatoms. Although a direct calculation of a force gradient map of the surface is not possible due to the computational cost, Figs. 3 and 8 show the direct proportionality between forces and gradients for large distances. It should be noticed that if a functional dependence such as the Morse potential is assumed, the behavior at large distances would be dominated by an exponential term, and the force gradient would be essentially the force multiplied by a constant factor. In the case of a power-law dependence (such as the one obtained, for example, for the VdW interaction), the gradient would be essentially the force divided by a factor proportional to the distance, which in a lateral scan at a constant height would again be a constant. Therefore using the lateral force scans we can map out the AFM “image” of the adatoms.

Lateral force and total-energy scans at a tip-surface distance of 5 Å are presented in Figs. 9 and 10. In Fig. 9 we show the total energy³² and the normal force for a tip scanning along the long diagonal and for a scan parallel to the long diagonal over the off-diagonal adatoms. Figure 10 shows the values of the forces calculated for a set of scans parallel to the long diagonal, which probe intermediate positions between the off-diagonal adatoms and the long diagonal. Each intermediate scan is 0.5 Å closer to the long diagonal, starting from the off-diagonal adatom scan, which is 3.84 Å off the long diagonal.

The differences between the scans over the diagonal and off-diagonal adatoms are related to a symmetry breaking distortion; there is a Jahn-Teller distortion that breaks the C_{3v} symmetry of the surface and leaves the off-diagonal adatoms at lower heights than the diagonal ones. A similar symmetry breaking was found in Ref. 39 for this reconstruction. In this respect, the behavior of the 5×5 reconstruction seems to be different from the one calculated for the 7×7 reconstruction using the same theoretical approach,^{40,41} where no distortion was found. This results in a different response of the adatoms in the two scans. The adatom response for the scan along the long diagonal can be seen in Fig. 11, which shows that as the tip approaches the diagonal adatom in one half of the unit cell this adatom moves upwards and electronic charge is transferred into the dangling bond of that adatom, while at the same time the adatom in the other half of the unit cell moves downwards and its dangling bond is depleted of charge. As the tip reaches the point midway between the adatoms, both of them have come back to their original po-

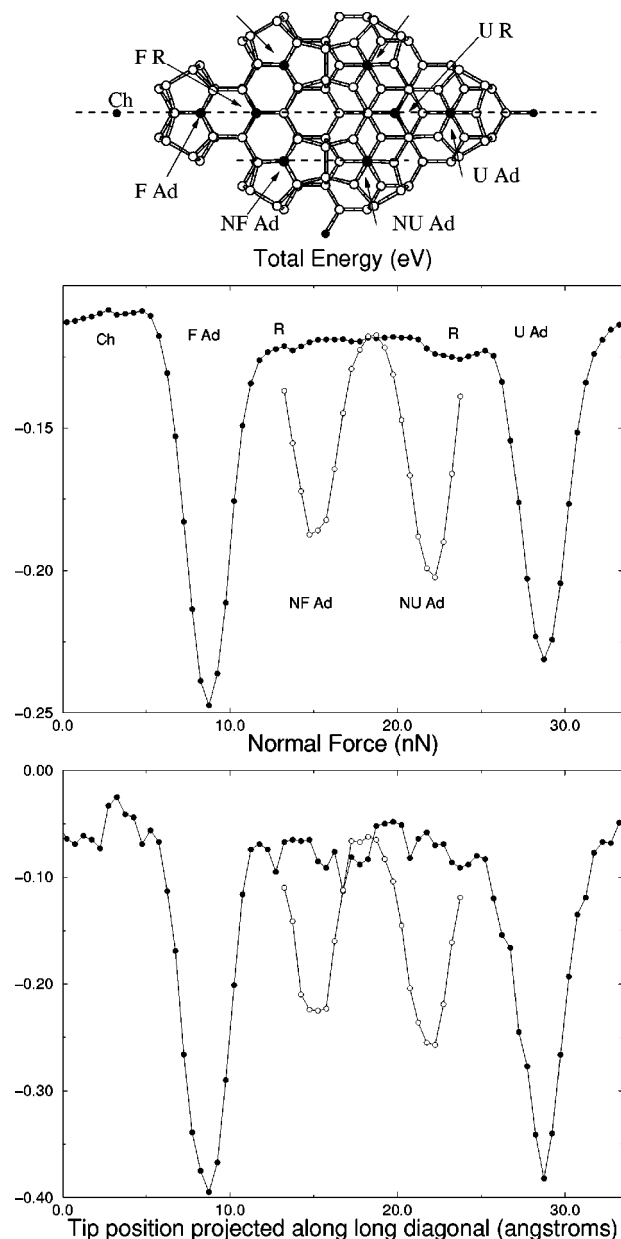


FIG. 9. Short-range interaction energy (eV, medium panel) and force (nN, bottom panel) for tip (c) of Fig. 1 scanning over the long diagonal (black circles) and for a scan parallel to the long diagonal over the off-diagonal adatoms (white circles) at a tip-surface distance of 5 Å. The labels indicate the position of the atoms with dangling bonds on the surface (F Ad, U Ad, R, Ch, NF Ad, and NU Ad). The top panel shows the two scans on a top view of the unit cell of the 5×5 reconstruction.

sitions, and the process reverses with the faulted adatom moving upwards and taking charge, as the tip approaches this adatom. The normal displacements of the adatoms are very different for the diagonal and off-diagonal scans and this is reflected in differences in the strengths of the concomitant tip-surface covalent bonds that are formed. We note that adjustment of the adatom-apex distance to the same value yields energies and forces that are identical for the two different scans. The interaction between dangling bonds on the adatoms and the dangling bond on the apex atom gives deep minima in the total-energy curve over the adatoms and a barely detectable signal at the positions of the rest atoms.

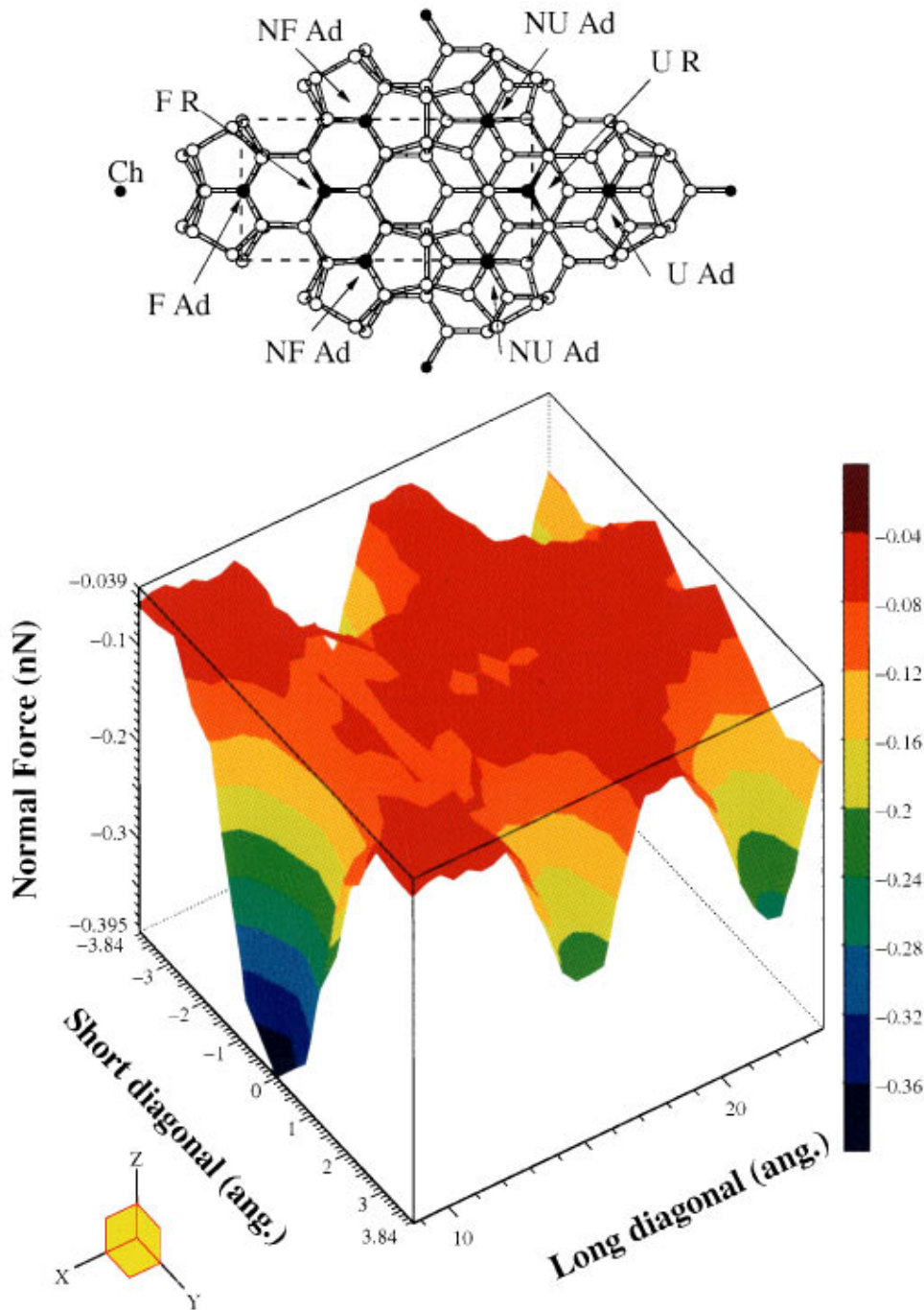


FIG. 10. (Color) Normal force (nN) for tip (c) scanning over an area of the unit cell (shown in the top panel) at a tip-surface height of 5 Å. The scan direction is parallel to the long diagonal. The minima correspond to the position of the adatoms, with the deeper one over the F Ad.

Similar results are obtained also for the normal force, albeit with an enhancement of the contrast so that the rest atoms are better resolved with the normal force. The differences between the faulted and unfaulted halves of the unit cell are in line with the different amount of charge in the dangling bonds in the two halves of the unit cell.⁴² The lowest binding energy and normal forces are obtained around the corner hole. From the half-width of the peaks in the force scans we estimate the lateral resolution of the order of ~ 3 Å. The calculations performed on the 3×3 structure³⁸ yield broadly similar results.

These results suggest that the tip may induce important long-range charge-transfer processes among the dangling bonds and backbonds that are directly correlated with the normal displacements of the surface atoms. This in turn can

be traced back to the way the tip interaction changes the relative contribution of the different dangling bonds on the surface to the electronic states close to the Fermi energy. When the tip is placed in a position midway between the two diagonal adatoms, our calculation shows four electronic states, associated with the different adatoms and the corner hole, within a region of ~ 0.1 eV around the Fermi energy. Below them, in a region of 0.2 eV, we find the states associated with the rest atoms. Two of the states associated to the adatoms (located at -0.018 and -0.089 eV with respect to the last occupied eigenstate) have a large weight on the faulted adatom. The charge densities associated with these states are shown in Fig. 12. These states show the faulted adatom dangling bond mixed with the dangling bonds from the unfaulted diagonal adatom, the corner hole and the non-

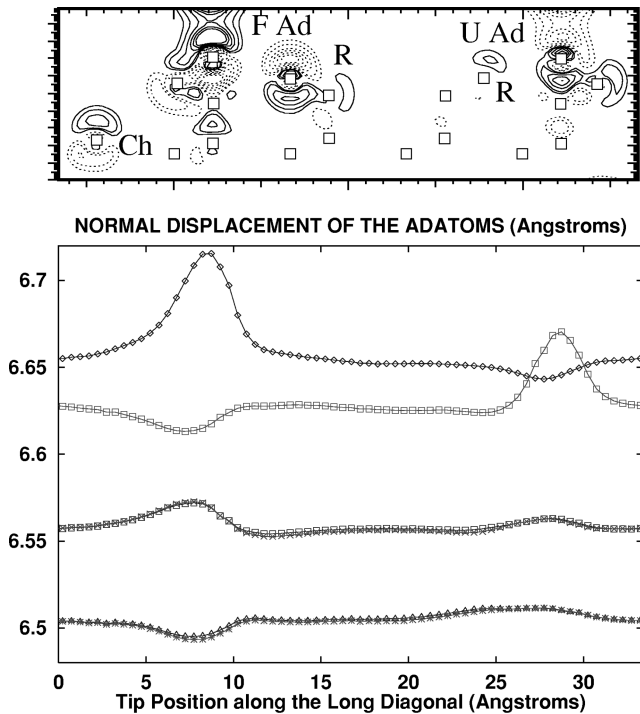


FIG. 11. Lower panel: normal displacements of the adatoms for tip (c) of Fig. 1 scanning over the long diagonal. The two upper curves correspond to the diagonal adatoms, the two intermediate to the off-diagonal faulted adatoms and the two lower to the off-diagonal unfaulted adatoms. Notice that the symmetry between the two halves of the unit cell is preserved during the scan. Upper panel: charge-transfer process accompanying the normal adatom displacements, charge-density difference between the self-consistent electronic density for the tip on the faulted and the unfaulted diagonal adatom (details as in Fig. 6, labels as in Fig. 9).

diagonal adatoms (not shown on the figure). A comparison with the local density of states obtained for the case where the tip is on top of the faulted adatom shows that the tip interaction singles out the faulted adatom from the rest of the adatoms and lowers these two states by 0.12 eV. The interaction (see Fig. 13) has removed the contributions from the corner hole and the other adatoms to these states and only a small contribution from the unfaulted diagonal adatom remains. The faulted adatom dangling bond now appears strongly mixed with the tip dangling bond and nonnegligible contributions from the rest atoms are observed due to the proximity in energy of those states.

IV. DISCUSSION AND CONCLUSIONS

We have presented above a detailed study of the tip-surface interactions involved in the noncontact AFM imaging of reactive surfaces. Our displacement curves show that for “near contact” distances (below 5 Å), the short-range covalent chemical bonding between the dangling bonds on the tip and the surface provides interaction energies and forces comparable to the macroscopic tip-surface VdW interaction, and completely dominates the force gradients probed by the experiments. More importantly, both the displacement curves and the lateral scans show that the covalent interaction has a strong dependence on the tip-surface distance and provides a clear contrast among different sites in the unit

cell. Thus, this interaction satisfies all the conditions for providing atomic resolution on reactive surfaces and for enhancing the resolution in other systems.

These conclusions have received a large amount of experimental support. The large differences in normal forces and force gradients between different atomic sites in the unit cell obtained in the simulations, with clear maxima over the adatoms, correlates with the contrast observed in all the experimental images taken in the constant frequency shift mode, where maxima in the tip height occur at the positions of the adatoms. Our finding of atomic resolution induced by tip-surface reactivity¹⁸ has recently been invoked to explain the observed differences in imaging inequivalent adatoms on the Si(111)-7×7 surface.⁹ Our present work lends further support to this interpretation. The discontinuity in the force gradient curve found on Si(111)-7×7 and its interpretation in terms of a crossover between van der Waals and chemical bonding^{6,11} is consistent with our results. The role of the dangling bond interactions is also supported by the experimental observation that the onset of tunneling current and the rapid variation of the frequency shift, recorded simultaneously in Ref. 7, take place at very similar tip-surface distances. Our displacement curves (see Sec. III A and Figs. 3 and 8) explain the difficulty in achieving stable operation in the frequency shift mode reported in early experiments. This is due to the change in slope of the normal force, and the associated change of sign for the force gradients, which takes place over a small range of distance.

Our results can also be used to discuss the quality of noncontact AFM images of Si(111)-7×7. The early image

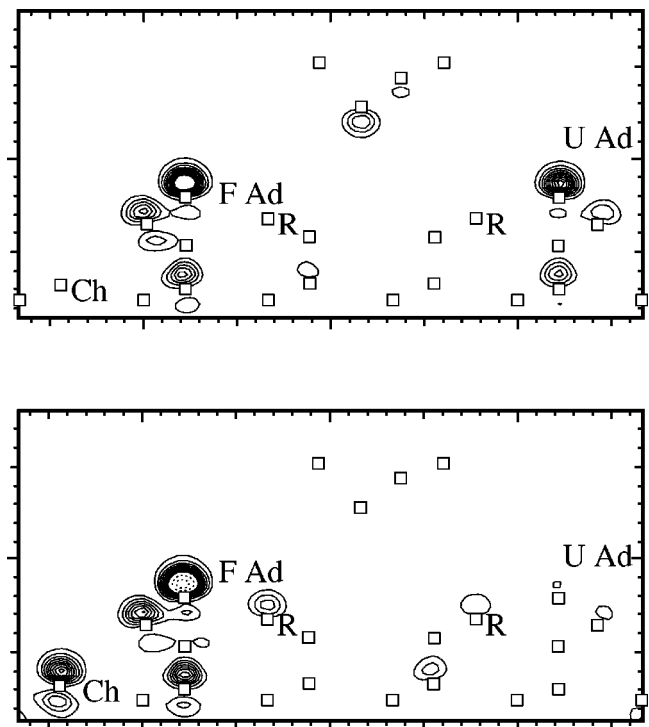


FIG. 12. Charge density associated with the two eigenstates closer to the Fermi energy, which have a larger weight on the faulted adatom. The tip is placed in a position midway between the two diagonal adatoms. The contours correspond to 0.2, 0.4, 0.6, 0.8, 1.0, 1.2, 1.4, 1.6, 1.8, 2.0 (continuous lines) and 3.0, 4.0, 5.0 (dashed lines) $\times 10^{-2}$ electrons/Å³.

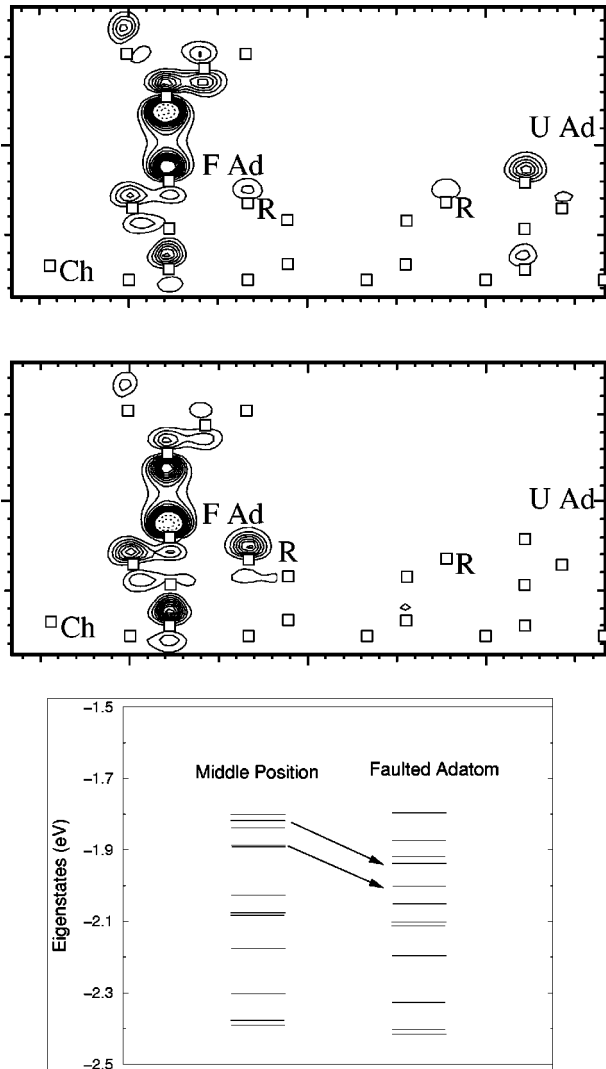


FIG. 13. As Fig. 12 when the tip is on top of the faulted diagonal adatom. The bottom panel shows the distribution of occupied eigenstates close to the Fermi level for the two positions of the tip, with the arrows marking the evolution of the two eigenstates considered in Fig. 12 and this figure.

of Giessibl² shows a low-quality image except for the width of one unit cell where the characteristic protrusions of the 12 adatoms suddenly appear and then disappear again. This effect could be induced either by pickup of a surface atom by the tip or by losing a contaminant previously attached to the apex of the tip apex. In either case, if a dangling bond pointing towards the surface is formed we would expect a dramatic improvement in resolution. A similar scenario is possible in the case of the metallic tip used in the damping experiments of Ref. 9, which provided images of extremely good quality. In the experimental setup of Kitamura and Iwatsuki,³ using a stiffer cantilever than Giessibl (37 N/m compared to 17 N/m) these processes are much less likely to happen and the original images were more fuzzy. However, a similarly dramatic improvement in resolution was achieved after tip depassivation.⁵ The tip depassivation is likely to expose the tip dangling bonds and so this change in experimental resolution could be due to the effects discussed in this paper.

A pronounced enhancement of the image contrast while

scanning with a Si tip on a Si(111)- 7×7 surface has been recently reported.¹¹ The enhancement correlates with the observation of a new type of force gradient curves which contain a discontinuity. Although, for the sake of brevity, we shall refer to these observed rapid changes in the force gradient as a discontinuity, it is necessary to point out that there are no real, physical force discontinuities. They are simply changes that occur over such a small distance as not to be resolvable in the experiment. In contrast to other experiments, the sample was prepared in this case in a different chamber to avoid the deposition of Si atoms on the tip apex. At the beginning of the AFM measurements only force gradient curves that did not have a discontinuity were observed. However, after accidental contact between the tip and the sample during the measurements force gradient curves with a discontinuity began to be observed. The discontinuity indicates a rapid increase of the attractive force acting on the tip which, as pointed out by the authors, can be naturally explained in terms of the onset of a chemical bonding interaction between the dangling bond out of the Si atoms picked up on the tip apex and the adatom dangling bond. In addition to the previous evidence that tip happens to pick up Si atoms from the surface,⁴³ atomic-scale removal of Si adatoms is actually observed in this experiment. It should be noticed that the contrast enhancement in the scans is mainly due to the discontinuity in the interaction, with the dark parts of the image corresponding to the smaller (lower) value of the force gradient below the discontinuity and the bright ones to the larger (upper) value. This is consistent with the stronger interaction due to the onset of covalent bonding occurring over the adatoms and the much weaker interaction occurring over the rest atoms and the corner hole as we obtain in our simulations.

The model we considered here is in many respects an oversimplification. In particular, we consider only tips with a single unsaturated dangling bond, scanning a perfect surface parallel to the long diagonal at a constant height. Despite all these simplifications our model yields energies, forces and force gradients that are qualitatively comparable to the estimated experimental values. For example, the short-range normal forces shown in Fig. 9 are comparable to estimated experimental force of -0.14 nN (Ref. 2) and the calculated force gradient of ~ 10 N/m at over the adatoms is close to the force constant of the piezolever (17 N/m) in that experiment making the scenario of an accidental tip-surface contact and the concomitant apex atom pickup quite likely.

A direct quantitative comparison of calculated force gradients and measured frequency shifts is still precluded by the complicated dynamics of the cantilever: noncontact measurements often use a large amplitude of oscillation of the tip so the force due to interaction with the surface acts on the tip for only a small part of the oscillation cycle and the change in frequency is relatively small. It is worth noting, however, that the ratio between the force gradients calculated for the tips with and without dangling bonds is roughly the same as the ratio between the frequency shifts measured during lateral scans for the tips with and without a discontinuity in their force gradient curves.¹¹ Recently Giessibl has used canonical perturbation theory to derive an analytical expression for the frequency change due to tip-sample forces which can be described by an inverse power law.⁴⁴ This opens the pos-

sibility to determine the frequency change due to the vdW interaction—which is naturally described by these inverse power laws—and to estimate the contribution to the frequency change coming from the chemical bonding forces using a simple Lennard-Jones pair potential to describe the bonding interaction. After setting the parameters for the Lennard-Jones potential using the bulk silicon properties, he has fitted the theoretical frequency change to different experimental results in the literature, assuming a pyramidal tip and using as a fitting parameter $\tan^2(\alpha/2)A_H$, with α the tip angle and A_H the Hamaker constant. The fitted theoretical curves provide a reasonable description of the experimental data over a range of distances. In particular, they confirm the pronounced effect of the chemical forces on the frequency shift at tip-sample distances around 5 Å in the experiments with Si tips and Si(111) surfaces. These chemical bonding forces are responsible for the important departure from the behavior associated with a pure VdW interaction observed in the experiments and qualitatively described by the simplified model for covalent bonding included in the theoretical curve.

On the other hand, our estimates for the forces and force gradients differ by about an order of magnitude from those obtained in AFM spectroscopy experiments¹² even at the heights where the short-range chemical interactions should dominate. One possible explanation for these discrepancies might be the difficulty in relating the measured frequency shifts with the force gradients pointed out above. Some of these effects might be addressed experimentally and/or by refinement of our present model. Application of the theory to other systems studied experimentally, such as the InP(110) surface are under way.

ACKNOWLEDGMENTS

The calculations were performed on the JRCAT super-computer system. This work was partly supported by the New Energy and Industrial Technology Development Organization (NEDO). R.P. acknowledges financial support from the HCM Program (European Union) under Contract Nos. ERBCHBICT30779 and ERBCHRXCT930369, and from the CICYT (Spain) under Project No. PB92-0168.

APPENDIX A: CONVERGENCE TESTS

We have performed several tests for both the 3×3 and the 5×5 reconstructions in order to check the accuracy of our calculations with respect to the \bar{k} -point sampling and the energy cutoff used. These tests support the main conclusion of our paper: the strong contrast found in both the total

TABLE II. \bar{k} -point sampling convergence of the total energy and normal force for the interaction of a 4 Si atom tip [tip (b) in Fig. 1] on two positions on the Si(111)- 3×3 surface.

	Adatom	Mid position
Energy (Γ)	-0.088 eV	-0.020 eV
''(3k points)	-0.142 eV	-0.041 eV
Force (Γ)	-0.194 nN	-0.013 nN
''(3k points)	-0.322 nN	-0.017 nN

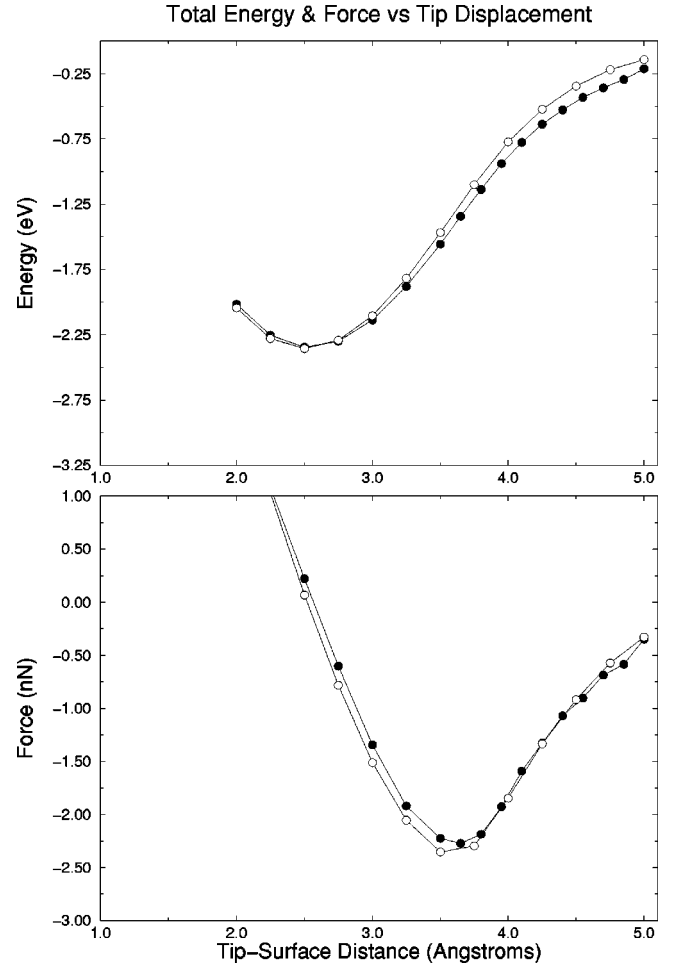


FIG. 14. Short-range interaction energy (top panel) and force (bottom panel) for tip (c) of Fig. 1 over an adatom on the 5×5 reconstruction (black circles) and tip (b) on the 3×3 reconstruction (white circles).

energy and the normal force between the adatoms and other positions in the unit cell is due to the onset of a covalent chemical interaction between the tip- and adatom-dangling bonds. In summary, test calculations at 11 Ry for the 5×5 reconstruction with the 10 Si atom tip [tip (c) in Fig. 1] show a very small reduction in the corrugation both in the energy (by 0.001 eV) and the normal force (by 0.012 nN) with respect to the 7-Ry cutoff used in the calculations presented above, and further tests at 20 Ry on the 3×3 reconstructions confirm these findings with reductions of 0.016 eV and 0.026 nN. Tests on the 3×3 reconstruction show that the apparent corrugation increases with the accuracy of the \bar{k} -point sampling and, with a slightly higher sampling density than used in the 5×5 calculations, gives results that are very similar to those presented above. What follows is a more detailed account of these tests.

1. \bar{k} -point sampling tests

The interaction of the Si(111)- 3×3 surface with a 4 Si atom tip with a dangling bond pointing out of the apex atom [tip (b) in Fig. 1] has been calculated using the same 7-Ry cutoff and two different sets of points: one set is just the Γ point, while the other contains three \bar{k} points: (0, 1/3),

TABLE III. Cutoff convergence of the total energy and normal force for the interaction of a 10 Si atom tip [tip (c) in Fig. 1] on two positions on the Si(111)- 5×5 surface.

	Adatom (faulted)	Mid position
Energy (7 Ry)	-0.129 eV	0.000 eV
(11 Ry)	-0.128 eV	0.000 eV
Force (7 Ry)	-0.395 nN	-0.052 nN
(11 Ry)	-0.402 nN	-0.071 nN

($1/3, 0$), and ($-1/3, 1/3$). We have fully relaxed the structure for two different positions of the tip: on top of one of the adatoms (the one in the unfaulted half of the unit cell in a position midway between the adatoms on the long diagonal). The convergence to the equilibrium configuration was performed with the same criteria as in the rest of our calculations, in particular, so that the forces on individual atoms were all less than 0.01 eV/Å. We have also calculated the surface and tip total energies with the same \bar{k} -point sampling to get the proper reference for the total energy of the interacting system.

Our results are summarized in Table II. Both the total energy and the normal force show that the corrugation increases significantly when we use the denser sampling. The results for this improved sampling are very close to the ones obtained for the 5×5 reconstruction using the Γ point only interacting with the same tip (-0.23 eV and -0.34 nN for the diagonal adatom on the unfaulted half of the unit cell). Adatom displacements also compared very well with the values obtained in the 5×5 reconstruction. Displacement curves (see Fig. 14), with the denser sampling for the 3×3 and Γ only for the 5×5 , provide very similar results, further confirming the accuracy of the Γ sampling for the 5×5 .

2. Energy cutoff tests

We have performed a full relaxation of the ionic coordinates for two different positions of the tip over the surface—on top of an adatom, and in a position midway between the adatoms on the main diagonal—for both the 3

TABLE IV. Cutoff convergence of the total energy and normal force for the interaction of a 4 Si atom tip [tip (b) in Fig. 1] on two positions on the Si(111)- 3×3 surface.

	Adatom (unfaulted)	Mid position
Energy (7 Ry)	-0.070 eV	0.000 eV
(11 Ry)	-0.052 eV	0.000 eV
(20 Ry)	-0.054 eV	0.000 eV
Force (7 Ry)	-0.194 nN	-0.013 nN
(11 Ry)	-0.194 nN	-0.015 nN
(20 Ry)	-0.178 nN	-0.023 nN

$\times 3$ and the 5×5 reconstructions. In the case of the 5×5 reconstruction we compare our results for the 7-Ry cutoff with the ones obtained using 11 Ry. For the 3×3 reconstruction we have also considered a 20-Ry cutoff. Γ sampling is used in all these calculations. In this case we have not calculated the energies of both the surface and the tip independently for each cutoff, so only differences in total energy between the two positions, taking the mid position as a reference, have been considered.

Our results are summarized in Tables III and IV. In the case of the 5×5 reconstruction there is a very small reduction in the corrugation both in the total energy and normal force. The change in the normal force is of the order of the convergence criteria for the individual forces on the equilibrium configuration. The 3×3 reconstruction shows a larger reduction in the corrugation when moving to the 20-Ry cutoff, but still exhibits a very clear contrast between the two positions of the tip. As both the 3×3 and 5×5 calculations show a similar trend when moving to larger cutoffs, we expect a similar behavior for the 5×5 system with a 20-Ry cutoff.

Finally, we have to mention that the structure and energetics of other silicon surfaces are well reproduced and practically converged with our optimized pseudopotential and the 7-Ry cutoff used in this work. As an example, our pseudopotential shows the correct buckling on the dimers of the Si(111)- 2×1 surface, a quantity that is not recovered by a standard (not optimized) pseudopotential until a cutoff larger than 12 Ry is used.

¹G. Binnig, C. F. Quate, and Ch. Gerber, Phys. Rev. Lett. **56**, 930 (1986).

²F. J. Giessibl, Science **267**, 68 (1995).

³S. Kitamura and M. Iwatsuki, Jpn. J. Appl. Phys., Part 1 **35**, L145 (1995).

⁴H. Ueyama, M. Ohta, Y. Sugawara, and S. Morita, Jpn. J. Appl. Phys., Part 1 **34**, L1086 (1995).

⁵S. Kitamura and M. Iwatsuki, Jpn. J. Appl. Phys., Part 1 **35**, L668 (1996).

⁶Y. Sugawara, H. Ueyama, T. Uchihashi, M. Ohta, Y. Yanase, T. Shigematsu, M. Suzuki, and S. Morita, in *Defects in Electronic Materials II*, edited by J. Michel, T. Kennedy, K. Wada, and K. Thonke, MRS Symposia Proceedings No. 442 (Materials Research Society, Pittsburgh, 1997).

⁷R. Lüthi, E. Meyer, M. Bammerlin, A. Baratoff, T. Howald, Ch.

Gerber, and H.-J. Güntherodt, Z. Phys. B **100**, 165 (1996).

⁸P. Güthner, J. Vac. Sci. Technol. B **14**, 2428 (1996).

⁹R. Erlandsson, L. Olsson, and P. Mårtensson, Phys. Rev. B **54**, R8309 (1996).

¹⁰N. Nakagiri, M. Suzuki, K. Oguchi, and H. Sugimura, Surf. Sci. **373**, L329 (1997).

¹¹T. Uchihashi, Y. Sugawara, T. Tsukamoto, M. Ohta, S. Morita, and M. Suzuki, Phys. Rev. B **56**, 9834 (1997).

¹²S. P. Jarvis, H. Yamada, S.-I. Yamamoto, H. Tokumoto, and J. B. Pethica, Nature (London) **384**, 247 (1996).

¹³K. Takayanagi, Y. Tanishiro, M. Takahashi, and S. Takahashi, J. Vac. Sci. Technol. A **3**, 1502 (1984); Surf. Sci. **164**, 367 (1985).

¹⁴See, for instance, R. G. Parr and W. Yang, *Density-Functional Theory of Atoms and Molecules* (Oxford University Press, Oxford, 1989).

- ¹⁵S. Ciraci, E. Tekman, A. Baratoff, and I. P. Batra, Phys. Rev. B **46**, 10 411 (1992).
- ¹⁶S. Ciraci, A. Baratoff, and I. P. Batra, Phys. Rev. B **41**, 2763 (1990).
- ¹⁷J. Israelachvili, *Intermolecular & Surface Forces* (Academic, London, 1992), p. 176.
- ¹⁸R. Pérez, M. C. Payne, I. Štich, and K. Terakura, Phys. Rev. Lett. **78**, 678 (1997).
- ¹⁹M. C. Payne, M. P. Teter, D. C. Allan, T. A. Arias, and J. D. Joannopoulos, Rev. Mod. Phys. **64**, 1045 (1992).
- ²⁰A. Rappe, K. M. Rabe, E. Kaxiras, and J. D. Joannopoulos, Phys. Rev. B **41**, 1227 (1990).
- ²¹J. S. Lin, A. Qteish, M. C. Payne, and V. Heine, Phys. Rev. B **47**, 4174 (1993).
- ²²R. D. King-Smith, M. C. Payne, and J. S. Liu, Phys. Rev. B **44**, 13 063 (1991).
- ²³I. Štich, K. Terakura, and B. E. Larson, Phys. Rev. Lett. **74**, 4491 (1995).
- ²⁴I. Štich, J. Kohanoff, and K. Terakura, Phys. Rev. B **54**, 2642 (1996).
- ²⁵See, for instance, J. P. Perdew, J. A. Chevary, S. K. Vosko, K. A. Jackson, M. R. Pederson, D. J. Singh, and C. Fiolhais, Phys. Rev. B **46**, 6671 (1992).
- ²⁶J. A. White and D. M. Bird, Phys. Rev. B **50**, 4954 (1994).
- ²⁷L. J. Clarke, I. Štich, and M. C. Payne, Comput. Phys. Commun. **72**, 14 (1992).
- ²⁸E. Hult, Y. Andersson, B. I. Lundqvist, and D. C. Langreth, Phys. Rev. Lett. **77**, 2029 (1996).
- ²⁹T. J. Senden and C. J. Drummond, Colloids Surf., A **94**, 29 (1995).
- ³⁰U. Hartmann, Phys. Rev. B **43**, 2404 (1991).
- ³¹E. M. Lifshitz, Sov. Phys. JETP **2**, 73 (1956); I. E. Dzyaloshinskii, E. M. Lifshitz, and L. P. Pitaevskii, *ibid.* **37**, 161 (1960).
- ³²The zero of the energy was set to the sum of the total energies of the slab and the tip calculated independently in the same unit cell.
- ³³A. R. H. Clarke, J. B. Pethica, J. A. Nieminen, F. Besenbacher, E. Laegsgaard, and I. Stensgaard, Phys. Rev. Lett. **76**, 1276 (1996).
- ³⁴L. Olesen, M. Brandbyge, M. R. Sorensen, K. W. Jacobsen, E. Laegsgaard, I. Stensgaard, and F. Besenbacher, Phys. Rev. Lett. **76**, 1485 (1996).
- ³⁵R. Wolkow and Ph. Avouris, Phys. Rev. Lett. **60**, 1049 (1988).
- ³⁶L. Olsson, R. Wigren, and R. Erlandsson, Rev. Sci. Instrum. **67**, 2289 (1996).
- ³⁷P. Varshni, Rev. Mod. Phys. **29**, 664 (1957).
- ³⁸R. Pérez, M. C. Payne, I. Štich, and K. Terakura, in *JRCAT International Workshop on Atomically Controlled Surface Processes*, edited by K. Terakura and T. Uda, Tsukuba, Japan, 1995 (Augstrom Technology Partnership, Tokyo, 1996).
- ³⁹G. B. Adams and O. F. Sankey, Phys. Rev. Lett. **67**, 867 (1991).
- ⁴⁰I. Štich, M. C. Payne, R. D. King-Smith, J.-S. Lin, and L. J. Clarke, Phys. Rev. Lett. **68**, 1351 (1992).
- ⁴¹K. D. Brommer, M. Needels, B. E. Larson, and J. D. Joannopoulos, Phys. Rev. Lett. **68**, 1355 (1992).
- ⁴²R. J. Hamers, R. M. Tromp, and J. E. Demuth, Phys. Rev. Lett. **56**, 1972 (1986).
- ⁴³A. Kobayashi, F. Grey, R. S. Williams, and M. Aono, Science **259**, 1724 (1993).
- ⁴⁴F. J. Giessibl, Phys. Rev. B **56**, 16 010 (1997).